Electronic Supplementary Material (ESI) for Lab on a Chip.

Supporting information

of

Programmable microfluidic logic device fabricated with shape memory polymer

Sei Hyun Yang[a¶], Juhyuk Park[a¶], Jae Ryoun Youn[a*], and Young Seok Song[b*]

[a] Research Institute of Advanced Materials (*RIAM*), Department of Materials Science and Engineering, Seoul National University, Seoul 08826, Republic of Korea,

[b] Department of Fiber System Engineering, Dankook University, Gyeonggi-do, 16890, Republic of Korea.

[¶] These authors contribute equally to this study.

* Corresponding author: Jae Ryoun Youn

Tel.: +82-2-880-8326; *E-mail address*: jaeryoun@snu.ac.kr

and Young Seok Song

Tel.: +82-31-8005-3567; *E-mail address*: ysong@dankook.ac.kr

Numerical simulation

1. Shape memory-recovery simulation

Numerical analysis was performed to model the shape memory behavior of SMCPAc theoretically and to confirm stress distribution of the material during deformation. ABAQUS/CAE, a commercial finite element method program, was employed in the simulation with codded subroutines UMAT and SDVINI. A hyperelastic model, Neo-Hookean model, was a constitutive model of the material with assumptions that strain energy exists as a form of Helmholtz potential during deformation of the material and the material is isothermal and compressible.

The mechanism of a shape memory polymer is as follows. The strain energy is generated on the region that receives stress and stored during glass transition. Due to the increased stiffness of SMCPAc after the cooling process, SMCPAc maintains its deformed figure even after unloading. The following heating process restores the original shape of SMCPAc by lowering the stiffness through phase transition from glassy state to rubbery state.

Khanolkar *et al.*[58,59] proposed the hyperelastic model as follows and we referred their works to simulate our material. The material properties should be varied with temperature condition. Two parts of strain energy function (ψ), glassy phase parts (α) and rubbery phase parts $(1-\alpha)$, were simultaneously considered in modeling. Constitutive equations of SMCPAc were defined as

$$\psi_t = (1-\alpha)\psi_r + \int_{t_i}^{\tau} \psi_g d\tau \qquad (1)$$

$$\psi_r = C_{10}\left(\bar{I}_{\kappa_r} - 3\right) + \frac{1}{D_1}\left(J_{\kappa_r} - 1\right)^2 \qquad (2)$$

$$\psi_g = C_{20}\left(\bar{I}_{\kappa_{g(t)}} - 3\right) + \frac{1}{D_2}\left(J_{\kappa_{g(t)}} - 1\right)^2 \qquad (3)$$

, where ψ_t is the total stored strain energy function, ψ_r is the stored strain energy function at rubbery regions, ψ_g is the stored strain energy function at glassy regions, $\bar{I}_{\kappa_r}$ and $\bar{I}_{\kappa_{g(t)}}$ are the first invariants of isochoric parts of the right Cauchy-Green deformation tensor, and J_{κ_r} and $J_{\kappa_{g(t)}}$are the Jacobian matrices of material deformation. Subscripts ‘r’ and ‘g’ indicate the

properties about rubbery phase and glassy phase, respectively. $C_{10}(=\mu_r/2)$, $C_{20}(=\mu_g/2)$ are the material input parameters for hyperelastic models related to shear modulus (μ), and $D_1(=2/K_r)$, $D_2(=2/K_g)$ related to bulk modulus (K).

Above material functions are continuously updated following a change of phase states relevant with temperature condition. In the subroutine code, it was assumed that phase transition is linearly proportional to the glassy state fraction (α). Glassy region content (α) is governed by temperature variation as

$$\alpha = \frac{T_{rub} - T}{T_{gla} - T_{rub}} \tag{4}$$

, where T_{rub} is the temperature when fully rubbery state, T_{gla} is the temperature when fully glassy state, and T is the current temperature condition.

The UMAT subroutine code was produced to model the non-linear material behaviors of SMCPAc. Based on Kirchhoff stress-Newman strain rate, stiffness tensor matrix (C) was developed as

$$C_{IJ} = \frac{1}{2}(C_{ijkl} + C_{ijlk}) \tag{5}$$

$$C_{ijkl} = \left\{(1-\alpha)\left\{\left(\frac{2C_{10}}{J_{\kappa_a}}\right)\left(\delta_{ik}\bar{B}_{a_{ij}} + \bar{B}_{a_{ik}}\delta_{jl}\right) + \left(-\frac{4C_{10}}{3J_{\kappa_a}}\right)\left(\delta_{kl}\bar{B}_{a_{ij}} + \bar{B}_{a_{kl}}\delta_{ij}\right) + \left(\frac{4C_{10}}{9J_{\kappa_a}}\right)\right.\right. \tag{6}$$

, where δ_{ij} is Kronecker delta and $\bar{B}$ is the isochoric parts of deformation components for glassy and rubbery state. The UMAT code is invoked to update the stress and phase states of each node with a use of the SDIVINI code at the end of every time step. The material parameters required in the simulation were obtained from the experimental results of isothermal tensile tests at different temperatures as arranged in Supplementary information.

A 3-D model was built regarding the real channel geometry. If the simulation is performed with a structure that perfectly reflects the actual experimental conditions, an excessive number of meshes have to be generated for calculation since the channel is at microscale. Therefore, rather than considering the entire geometry, we constructed the structure of interest and investigated only that part. SMCPAc rectangular microchannel with aspect ratio of 4:1 was located above PDMS layer with the same thickness along y-direction (Figure S3). Two layers were merged like as one domain and 8 node linear brick meshes were generated for the calculation. The finer mesh was generated only along the edges of the channel in order to

prevent time-consuming process. An analytical rigid plate was described for loading boundary condition. The bottom of merged domain was pinned for all directions. The steps for the simulation were consist of loading, cooling, unloading, and heating. In the loading step, the glassy region content (α) was 0.125 at the temperature of 40℃. When the analytical rigid plate pressed the upper surface of SMCPAc part, 4:1 microchannel was distorted as the similar shape in the SEM image. The deformed shape was fixed at the cooling step (α=0.625). At the followed unloading step, the plate was slowly removed from the SMCPAc and PDMS layer was fully-recovered since it doesn't have shape memory function. Finally, the deformed SMCPAc microchannel shape was recovered at the heating step. The von Mises stress was contoured in Figure 3B.

2. Heat transfer analysis through PDMS film

In order to predict a temperature increase of the SMCPAc microchannel through the PDMS film on the ITO glass, heat transfer between the materials was theoretically calculated by using the commercial program COMSOL Multiphysics based on finite element method (FEM). The PDMS film was designed to have thickness of 1 mm. To solve the temperature distribution of the SMCPAc layer, the following governing equation was given.

$$\rho C_p \frac{\partial T}{\partial t} = \nabla \cdot (k \nabla T) + Q \qquad (7)$$

, where ρ is the density, C_p is the heat capacity, k is the thermal conductivity, and Q is the heat source. The input variables above were given as intrinsic material properties for each layer. The heat source (Q) was defined as P_b/A for the heating process, where P_b is the supplied power and A is the surface area of the layer. For the cooling process, the heat source was defined as zero. The convective heat flux condition was set as the boundary condition as follow.

$$q_0 = n_s \cdot k \nabla T = h \cdot (T_{ext} - T) \qquad (8)$$

, where n_s is the surface normal vector, h is the convective heat transfer coefficient, and T_{ext} is the external temperature.

3. Simulation of hydraulic pressure distribution in microchannel

Numerical simulation was carried out to analyze pressure difference of the deformed channel

cross-section by using the commercial program COMSOL Multiphysics based on finite element method (FEM). Since we used the polymer solution with viscoelastic properties, the first normal stress difference distribution ($^{N}1$) was also considered during the calculation.

For the simulation, the steady-state momentum equation of Navier-Stokes equations was expressed as

$$\rho\left(\frac{\partial u}{\partial t} + (u \cdot \nabla)u\right) = \nabla \cdot \left(- pI + \eta_s\left(\nabla u + (\nabla u)^T\right) + T\right) \qquad (9)$$

And the extra stress source was given by

$$T + \lambda\left(\frac{\partial T}{\partial t} + (u \cdot \nabla)T - [(\nabla u) \cdot T + T \cdot (\nabla u)^T]\right) = 2\eta_p\left(\nabla u + (\nabla u)^T\right) \quad (10)$$

, where $\boldsymbol{u}$ is the velocity vector, λ is the characteristic relaxation time, η_p and η_s are the viscosities of polymer and solvent, respectively, and the total viscosity (η) is defined as $\eta_p + \eta_s$. These two equations are solved together with the continuity equation of Navier-Stokes equations. The pressure and velocity fields were obtained for the cases of non-deformed and deformed channel cross-section.

Characterization

1. Thermomechanical properties of SMCPAc

Thermomechanical property of SMCPAc was investigated by running a dynamic mechanical analysis (DMA) machine (TA Q800 DMA, United States) as shown in Figure S4. The cut specimen to 1×5.3×40 mm^3 was held in the tensile mode clamp . Storage and loss modulus of the sample were examined under 0.2% strain, 1 Hz frequency, 125% force track, 0.001 N preload, and 5℃/min heating rate.

A cyclic stress-strain-temperature curve was obtained using the same machine, TA Q800 DMA. A 3-point-bending test was proceeded after holding the same specimen used in the tensile test. After heating the specimen above transition onset temperature (T_{onset}, 40℃ in our case), 2% strain was applied at the center of the specimen. After then, the specimen was cooled to 0℃ for shape-fixing. After unloading, the specimen was heated up to 40℃.

2. Rheological properties of PEO solution flow

Dilute polyethylene oxide (PEO) solution is used as a viscoelastic medium due to its viscous and elastic properties. The rheological properties of viscoelastic solutions, such as the steady shear viscosity (η) and the relaxation time (λ), are measured by using a rotational rheometer (MCR-301, Anton Paar) and a capillary breakup extensional rheometer (CaBER-1, ThermoHakke), respectively. In the previous study, the distance between the double particle focusing lines was closer as the concentration increase of PEO solution from 1500 ppm to 3000 ppm. Due to the channel geometrical features of y-shaped inlets, the particle equilibrium regions can be bifurcated. And it facilitates double-line particle focusing by the additional shear-gradient force. In order to generate high elastic force outweighing the inertial forces, 2500 ppm PEO solution was selected and the double line particle focusing was observed with the short distance between the focusing lines in the channel. Since the temperature of the deformed microchannel increased up to 40℃ in the shape-recovery process, the viscosity of 2500 ppm PEO solution was also measured at 40℃.

For the 2500 ppm PEO solution, the elastic force (*Wi*) is more dominant than the inertial force (*Re*) as elasticity ($El=Wi/Re=\frac{\lambda\eta(W+H)}{\rho W^2 H}$) becomes larger than unity. The Reynolds number(*Re)* is a dimensionless number that indicates the comparison of inertial and viscous

effects, which is defined as $Re = \frac{\rho u D_h}{\eta} = \frac{2\rho Q}{\eta(W+H)}$, where H is the channel height, W is the channel width, ρ is the fluid density, u is the fluid velocity, and $D_h = 2WH/(W+H)$ is the hydraulic diameter of the rectangular channel. The elastic force is described by the Weissenberg number, Wi, which is defined as $Wi = \lambda\dot{\gamma}_c = \frac{2\lambda Q}{HW^2}$, where $\dot{\gamma}_c$ is the shear rate. The fluid elasticity is characterized by the ratio of Re to Wi. In this study, the elasticity of the solution was calculated according to the temperature increase. The viscosities were measured by increasing the temperature by using a rotational bulk-rheometer MCR 301 (Figure S5). At room temperature, El is above the unity as 1.366. As the temperature increases up to 40℃, the elasticity decreased as 0.933 due to the decrease of the solution viscosity.

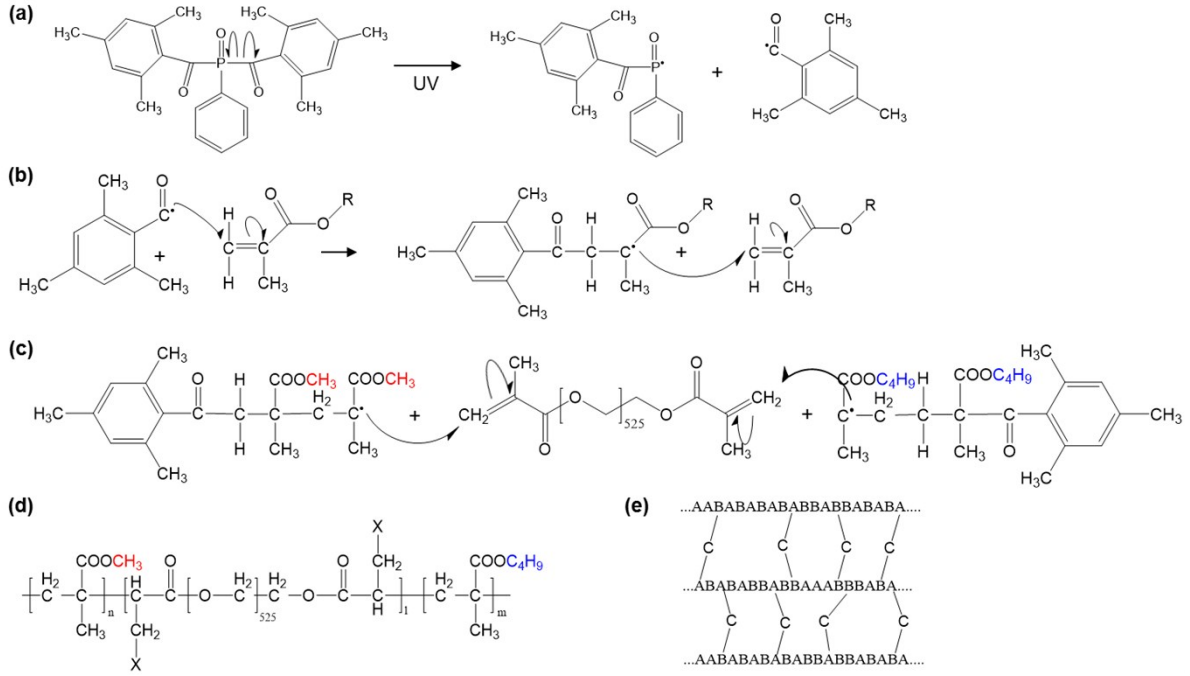

Figure S1. Chemical reaction scheme for SMCPAc synthesis. (a) Initiation of the reaction by irradiation of UV light. (b) Extension of the prepolymer chains by the generated free radical electrons. (c) Crosslinking reaction between the pre-polymer chains and the crosslinker. (d) Suggested chemical structure of the SMCPAc. (e) Schematic illustration of the SMCPAc consisted of the monomers ('A' and 'B' indicate MMA and BMA, respectively) and the crosslinker ('C' means PEGDMA).

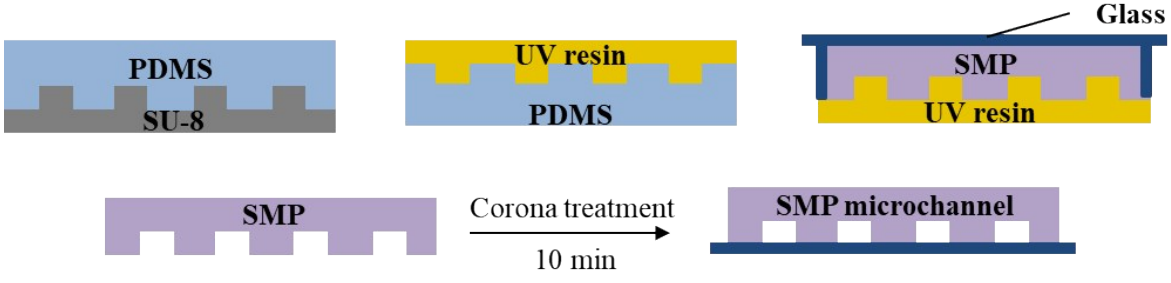

Figure S2. A schematic illustration for fabrication of SMCPAc microchannel.

Material properties for structural simulation

Table S1. The employed hyperelastic material parameters for SMCPAc.

	SMCPAc
T_r [a)] [°C]	60
T_g [b)] [°C]	-20
C_{10} [MPa]	6
C_{20} [MPa]	370
D_1 [1/MPa]	0.06
D_2 [1/MPa]	0.001
ν [c)] [-]	0.35

Table S2. The employed linear elastic material parameters for PDMS.

	PDMS
E [d)] [MPa]	13.2
ν [-]	0.45

a) T_r: Temperature for fully rubbery phase;
b) T_g: Temperature for fully glassy phase;
c) ν: Poisson's ratio.
d) E: Young's modulus;

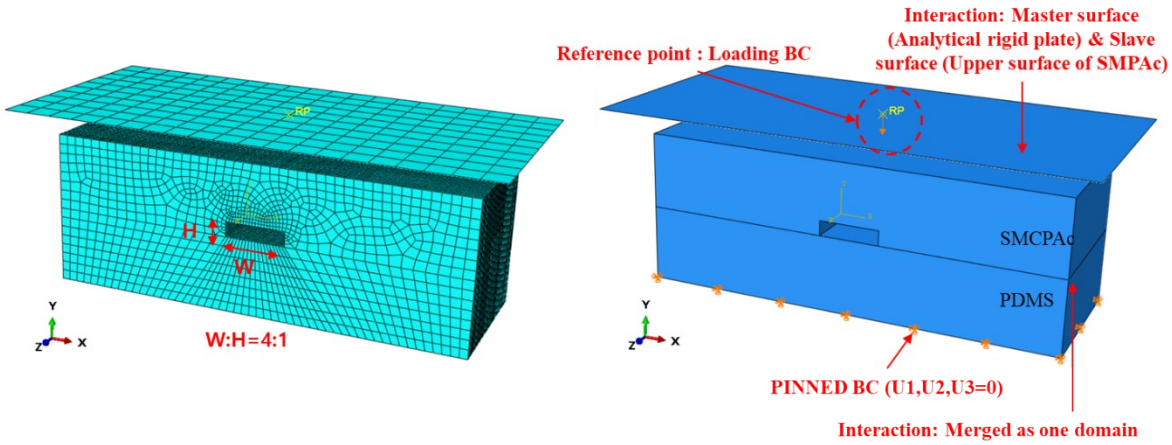

Figure S3. Geometrical design, mesh, and boundary condition for the structural simulation.

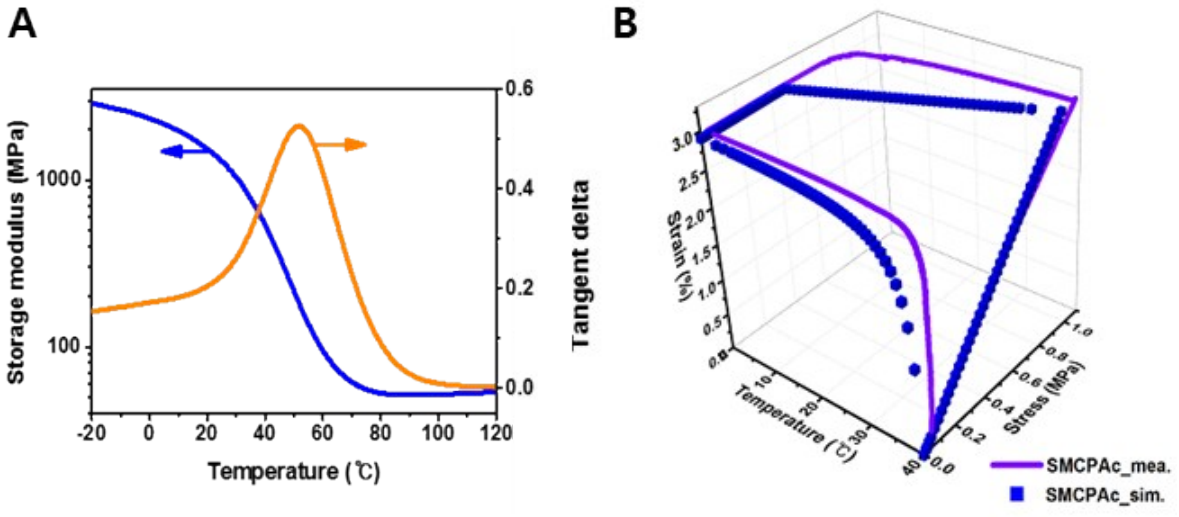

Figure S4. Thermomechanical analysis results for SMCPAc. (A) Storage modulus and tangent delta of the SMCPAc as a function of temperature. (B) Stress-strain-temperature curve for the SMCPAc.

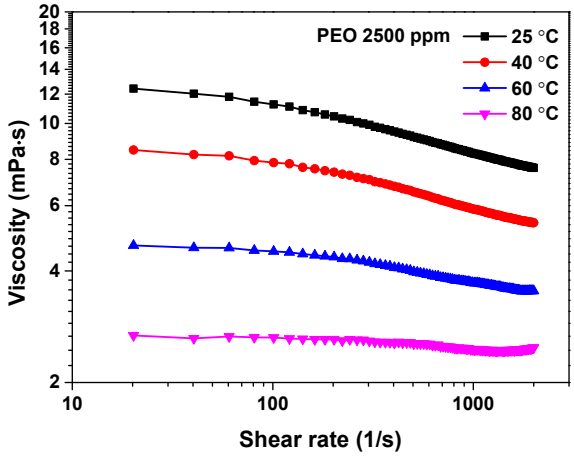

Figure S5. Viscosities of 2500 ppm Poly(ethylene oxide) aqueous solution measured at different temperature (25℃, 40℃, 60℃, 80℃).